

Not All Frame Features Are Equal: Video-to-4D Generation via Decoupling Dynamic-Static Features

Liyang Yang¹, Chen Liu², Zhenwei Zhu¹, Ajian Liu³, Hui Ma¹, Jian Nong¹, Yanyan Liang^{1†}

¹ Macau University of Science and Technology ² The University of Queensland

³ Institute of Automation, Chinese Academy of Sciences (CASIA)

† Corresponding Author

lyyang69@gmail.com

yyliang@must.edu.mo

Abstract

Recently, the generation of dynamic 3D objects from a video has shown impressive results. Existing methods directly optimize Gaussians using whole information in frames. However, when dynamic regions are interwoven with static regions within frames, particularly if the static regions account for a large proportion, existing methods often overlook information in dynamic regions and are prone to overfitting on static regions. This leads to producing results with blurry textures. We consider that decoupling dynamic-static features to enhance dynamic representations can alleviate this issue. Thus, we propose a dynamic-static feature decoupling module (DSFD). Along temporal axes, it regards the portions of current frame features that possess significant differences relative to reference frame features as dynamic features. Conversely, the remaining parts are the static features. Then, we acquire decoupled features driven by dynamic features and current frame features. Moreover, to further enhance the dynamic representation of decoupled features from different viewpoints and ensure accurate motion prediction, we design a temporal-spatial similarity fusion module (TSSF). Along spatial axes, it adaptively selects a similar information of dynamic regions. Hinging on the above, we construct a novel approach, DS4D. Experimental results verify our method achieves state-of-the-art (SOTA) results in video-to-4D. In addition, the experiments on a real-world scenario dataset demonstrate its effectiveness on the 4D scene. Our code will be publicly available.

1. Introduction

Generating dynamic 3D (4D) content [2–9] from video is an essential research topic involving the field of computer vision and computer graphics. However, it is rather formidable to predict accurate motion from a few view-

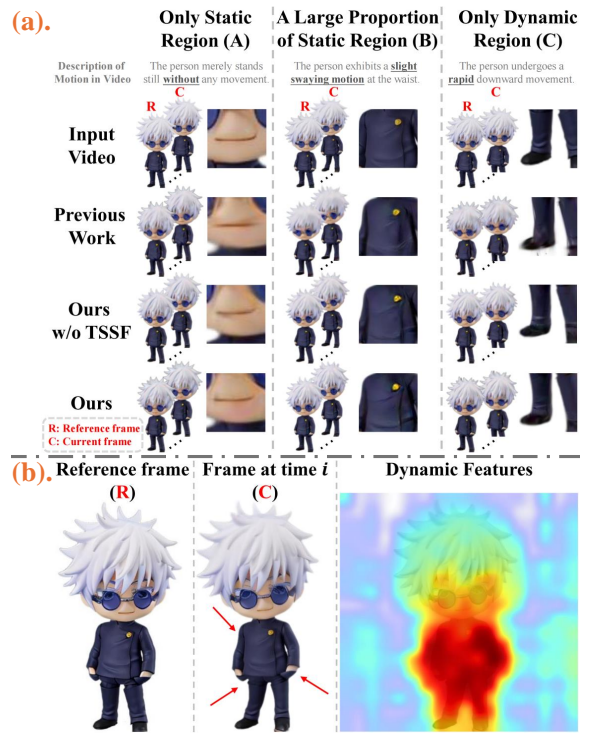


Figure 1. (a) Illustration of the issues caused by different proportions of dynamic and static regions. Previous work [1] generates the 4D content with obviously blurry textures in the dynamic regions with B-type video input. In contrast, our methods with decoupling dynamic-static features generates high-quality results with clear textures. (b) The visualization of dynamic features in our method. The red region highlights the primary region of interest in the dynamic features in B-type videos. This part is also the dynamic region between frames R and C. It demonstrates our method can successfully decouple dynamic-static features.

points while ensuring high-quality generation.

There are two main streams in current approaches to improving generation quality. Inference-based methods

[10–13] can generate high-quality 4D content by capturing temporal-spatial correlations in its 4D diffusion model. Another stream is optimization-based methods [1, 14–16]. These methods generate 4D content through distilling spatial prior knowledge from pre-trained multi-view [17, 18] diffusion models. However, the above methods only model temporal-spatial correlations using whole information in frames, but fail to explicitly differentiate between the dynamic and static regions of the frame. If static regions account for a significant portion, these models overlook dynamic information. Thus they tend to overfit static regions, resulting in a diminished capacity to perceive texture variations in dynamic zones. As shown in Fig.1 (a), the previous work (STAG4D [1]) produces results with blurred texture details (e.g., wrinkles in clothes), particularly when confronted with B-type input video.

To tackle above problems, we present a novel approach DS4D, which decouples dynamic and static features along temporal and spatial axes to enhance dynamic representations for high-quality 4D generation. In particular, we propose dynamic-static feature decoupling module (DSFD) to obtain decoupled features. We assume some portions of current frame features exhibit significant differences relative to reference frame features. Such portions always contain important knowledge of texture variations and motion trends under current timestamps. Therefore, it can be regarded as the dynamic feature of the current frame. In contrast, the remaining parts are the static features. Based on this assumption, we decompose the dynamic components between each frame feature and reference frame features along the temporal axes. The dynamic component (also termed dynamic features), as difference features between two frame features, is able to represent the dynamic information (as shown in Fig.1 (b)). At last, we acquire decoupled features driven by dynamic components and corresponding frame features.

Note that spatial occlusion results in the inability of dynamic components captured from a specific viewpoint to inadequately represent the authentic dynamic information in 4D space. To mitigate this issue, we design temporal-spatial similarity fusion module (TSSF) which engages in enhancing dynamic representations in features. The Gaussian points are initialized by utilizing a large reconstruction model [19]. Then, point features are obtained by retrieving decoupled features for Gaussian points via view projection in TSSF. Subsequently, TSSF produces fused Gaussian features by adaptively selecting information on dynamic regions containing similar texture, shape, and motion representations from point feature space at same timestamps along spatial axes. Finally, fused Gaussian features with strong dynamic representation, are used for 4D generation.

The contributions can be summarized as follows:

- We propose a novel framework DS4D, which decouples dynamic-static information along temporal-spatial

axes to enhance dynamic representations for high-quality 4D content generation.

- Leveraging significant differences between frame features, we propose dynamic-static feature decoupling module (DSFD) to decouple dynamic and static features.
- We tackle the issue of inadequate dynamic information in 4D space resulting from spatial occlusion by designing temporal-spatial similarity fusion module (TSSF). TSSF enhances dynamic representations in features.
- Experimental results on Consistent4D dataset [20] and Objaverse dataset [21] demonstrate our DS4D outperforms other SOTA methods in terms of video quality, motion fidelity, and temporal-spatial consistency. Furthermore, the experiments on a real-world scenario dataset [2] verify its effectiveness on 4D scenes.

2. Related Works

2.1. 3D Generation

3D generation aims to produce 3D assets using images or text descriptions. The early works generate 3D objects in voxels [23–26], meshes [27–29] or point clouds [30–32] forms. Recently, thanks to the popular application of NeRF [33, 34] and 3D Gaussian Splatting [35, 36], and the successful pre-trained text-to-image diffusion model [37] in 2D generation tasks, most works including DreamFusion [38] Dreamgaussian [39] that focus on 3D generation try to use Score Distillation Sampling (SDS) loss [38] to explore the possibility of inspiring potential 3D-aware from diffusion. However, these works always suffer from over-saturation, over-smoothing, and multi-face problems. Because it is a challenge to distill the invisible views while ensuring multi-view consistency based on 2D diffusion. In contrast, Zero-1-to-3 [17] and Zero123++ [18] directly train a 3D-aware diffusion model using multi-view images and corresponding camera poses. Zero-1-to-3 and Zero123++ usually generate more stable and high-quality novel views thanks to the spatial perception built into them. Therefore, in our method, we use Zero123++ to predict the novel views at all timestamps to provide additional multi-view sequences for optimization.

2.2. 4D Generation

Compared to 3D generation, 4D generation is a more challenging task. Current 4D representations are two main streams, including NeRF-based [5, 33, 40–43] and 3D Gaussians-based [8, 9, 35, 44–47]. Consistent4D [20], as the NeRF-based method, leverages the prior knowledge from pre-trained 2D diffusion models to optimize dynamic NeRF

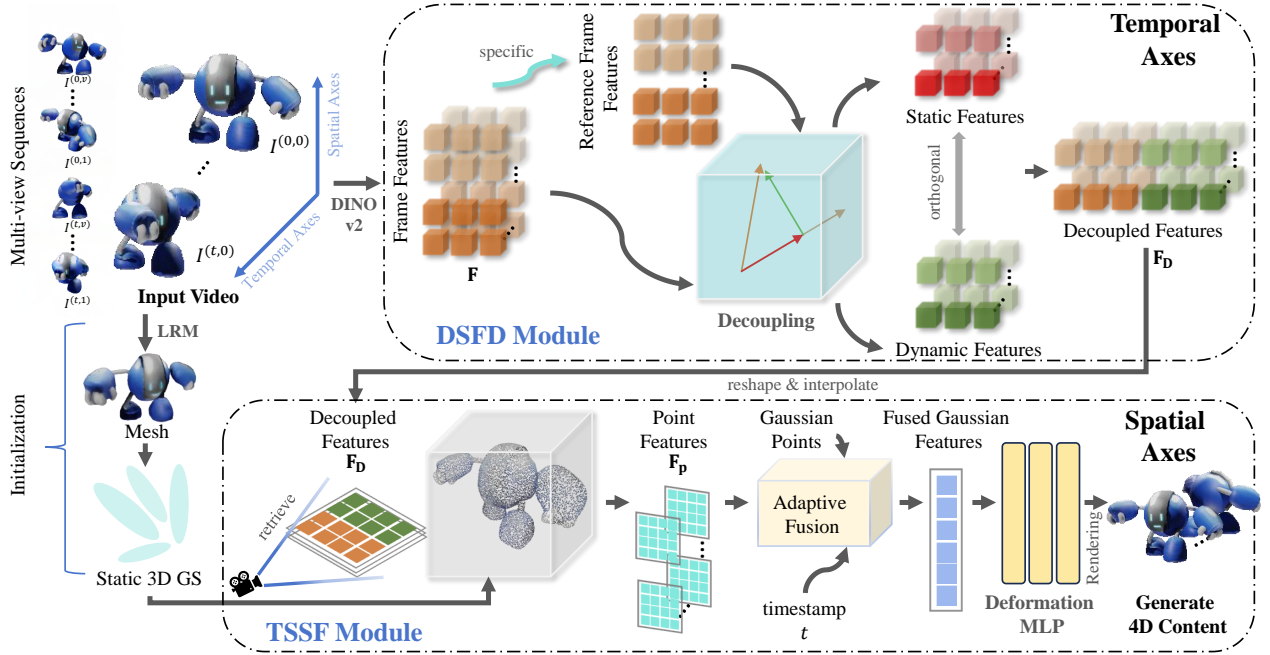


Figure 2. Overview of our proposed DS4D. Given an input video and corresponding multi-view sequences, our DS4D decouples features of the frame at time t based on the reference frame in DSFD module. Next, we acquire point features by retrieving each decoupled feature for Gaussian points via view projection, and we obtain fused Gaussian features by adaptively selecting similar dynamic information from point feature space in TSSF module. Finally, through Deformation MLP, our method generates 4D content. During the process, we utilize DINOv2 [22] to extract each frame feature and use a large reconstruction model (LRM) [19] to generate the corresponding mesh. We perform uniform sampling on the mesh to obtain point clouds. The point clouds are the initialization of static 3D Gaussian points.

by Score Distillation Sampling (SDS) optimization. Dreamgaussian4D [48], STAG4D [1] and SC4D [16] both attempt to introduce dynamic 3D Gaussians in 4D generation. Dreamgaussian4D notably reduces the cost of optimization time by improving the training strategies. STAG4D can generate anchor multi-view videos for optimization via a training-free strategy. SC4D optimizes sparse-controlled dynamic 3D Gaussians through SDS loss. However, these methods model temporal-spatial correlations using whole video but ignore the dynamic information in frames when static regions account for a large portion. It leads to them easily overfitting on static parts.

3. Method

3.1. Overview

In this section, we provide an overview of DS4D, which includes initialization in Sec.3.2, dynamic-static feature decoupling (DSFD) in Sec.3.3, and temporal-spatial similarity fusion (TSSF) in Sec.3.4. The overall framework of our proposed method is illustrated in Fig.2.

3.2. Initialization

Formally, we begin with a single-view video. For each frame in the video, we adopt Zero123++ [18] to infer the

pseudo multi-view images of frames. Then we obtain frame sequences, $\mathbf{I} = \{I^{(0,0)}, I^{(0,1)}, \dots, I^{(i,j)}, \dots, I^{(t,v)}\}$, where t represents the number of frames, and v represents the number of views of each frame.

Frame Feature Extraction. The frame features extracted by a visual foundation model must incorporate structural information, thereby ensuring that the information contained within the corresponding features is utilized to decouple the dynamic and static features. Recent research [49] demonstrates DINOv2 [22] has a stronger ability to capture the structure of input image than other foundation models [50, 51]. Therefore, we leverage DINOv2 to extract frame features $\mathbf{F} = \{f^{(0,0)}, f^{(0,1)}, \dots, f^{(i,j)}, \dots, f^{(t,v)}\}$ from sequences $\mathbf{I} = \{I^{(0,0)}, I^{(0,1)}, \dots, I^{(i,j)}, \dots, I^{(t,v)}\}$, where $f^{(i,j)} \in \mathbb{R}^{P \times D}$, P and D are the number of tokens and token dimension, respectively. Each feature $f^{(i,j)}$ encodes the geometry and texture of the corresponding frame.

Gaussian Points Initialization. Previous works usually randomly initialize Gaussian points, resulting in unstable topology during optimization. It ultimately affects the quality of the results. Considering the above problem, we generate the point clouds from the frame at middle timestamp by using a large reconstruction model [19], which is the initialization of static 3D Gaussian points. The initialization approach provides geometric prior and ensures the stability

of subsequent optimization.

3.3. Dynamic-Static Feature Decoupling (DSFD)

Now, we obtain frame features \mathbf{F} which include the features of all frames and their corresponding multi-view features. Then, we start from the following two aspects to decouple dynamic-static features: 1) Which frame features are regarded as references; 2) How to decouple frame features along temporal axes.

Which frame features are regarded as references? In order to support the model stably predict 4D contents, the decoupled dynamic information should precisely represent the variations in motion of the current frame relative to the entire video stream. Therefore, it is essential to define the reference frames employed to decouple the motion deformation between the current frame and reference frames. The most direct way is to treat each frame feature as a reference and decouple the dynamic and static features between references and other frame features one by one under different viewpoints along the temporal axis. However, it usually consumes considerable computation time.

To alleviate this issue, we sample reference frame features from \mathbf{F} and decouple features based on the current frame and reference frame features. This manner greatly reduces the computation time. Concretely, the frame $f^{(\frac{t}{2},j)}$ of middle timestamp and \dagger average frame features $\bar{f}^{(\bar{t},j)}$ are regarded as references. For frame $f^{(i,j)}$ at timestamp i , under viewpoint j , we can calculate the difference information of $f^{(i,j)}$ relative to $f^{(\frac{t}{2},j)}$ and $\bar{f}^{(\bar{t},j)}$. Based on the difference information, we decouple the dynamic and static features.

How to decouple frame features? To obtain decoupled features, we propose the dynamic-static feature decoupling module (DSFD). In DSFD, we aim to calculate differences by effectively utilizing both geometric and texture information present in features while maintaining the original distribution of pre-trained DINOv2 model. To achieve this, we implement a parameter-free architecture for decoupling.

The parameter-free decoupling architecture is shown in Fig.3. Specifically, given specific j -th view in timestamp i , we perform the projection of frame features $f^{(i,j)}$ onto reference frame features r^j . Actually, the projection serves as the component with similar information between the two frame features. The similar feature zones belong to the regions where there are no texture and shape variations between the two frames. Thus, the component can represent static features. Formally, for each frame feature $f^{(i,j)}$, the static features become:

$$f_{\text{static}}^{(i,j)} = f^{(i,j)} \cdot r^j \frac{r^j}{\|r^j\|_2^2}, \quad (1)$$

\dagger Average frame features $\bar{f}^{(\bar{t},j)}$ are derived from the average of all frame features from a particular view.

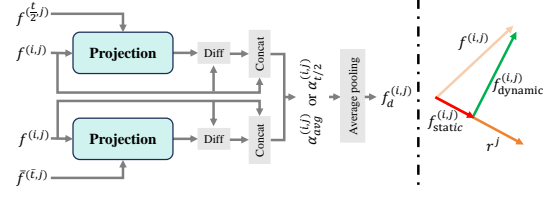


Figure 3. An overview of the decoupling architecture in DSFD. The decoupling architecture is shown on the left. The demonstration of projection is shown on the right.

where $f^{(i,j)} \cdot r^j = |f^{(i,j)}| \times |r^j| \times \cos(\theta)$, and θ is included angle between $f^{(i,j)}$ and r^j . Through projection, we obtain static features that exhibit the same geometric and texture information between current frame and reference frames.

We calculate the differential between current frame features and static features to achieve dynamic features (also termed dynamic components):

$$f_{\text{dynamic}}^{(i,j)} = f^{(i,j)} - f_{\text{static}}^{(i,j)}. \quad (2)$$

The dynamic features possess significant difference information, which represent the motion knowledge of the current frame relative to the reference frame. Therefore, we leverage dynamic features to enhance the dynamic representations in the current frame. In particular, for each type of reference frame features r^j , including $f^{(\frac{t}{2},j)}$ and $\bar{f}^{(\bar{t},j)}$, we perform eq. (1), eq. (2) to obtain corresponding dynamic features $f_{\text{dynamic}}^{(i,j)}$ at each timestamp. Afterwards, we append to each token of current frame features $f^{(i,j)}$ with dynamic features $f_{\text{dynamic}}^{(i,j)}$. The appended features are $\alpha_{t/2}^{(i,j)}$ and $\alpha_{avg}^{(i,j)}$. Last, we calculate the average pooling between the two features and acquire features $f_d^{(i,j)}$ with rich dynamic representations. We integrate all the features obtained based on both temporal and spatial axes into decoupled features $\mathbf{F}_D = \{f_d^{(0,0)}, f_d^{(0,0)}, \dots, f_d^{(i,j)}, \dots, f_d^{(t,v)}\}$.

3.4. Temporal-Spatial Similarity Fusion (TSSF)

After we get decoupled features \mathbf{F}_D , we have to enhance dynamic representations further. Because the dynamic features obtained from a particular viewpoint do not adequately represent the complete dynamic information in the 4D space. Thus, we design temporal-spatial similarity fusion module (TSSF) to select similar dynamic information from decoupled features at the same timestamp.

Inspired by [52], we retrieve decoupled features from Gaussian points by view projection. In particular, decoupled features are integrated into point features based on the given camera pose. The Gaussian points are well-aligned with decoupled features thanks to the projection operations.

Afterwards, we extract point features $\mathbf{F}_p = \{f_p^{(0,0)}, f_p^{(0,1)}, \dots, f_p^{(i,j)}, \dots, f_p^{(t,v)}\}$ which encapsu-

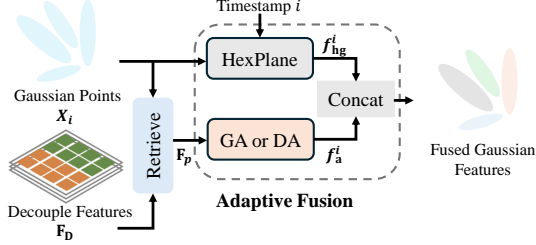


Figure 4. An overview of adaptive fusion in TSSF.

late extensive dynamic information. Among different viewpoints, we consider the texture, shape, and motion representations from point features to be similar for the same spatial area of the object in the frame. Hence, utilizing the similarities in information across viewpoints and aggregating them contributes to the enhancement of dynamic representations. According to the assumption, we propose an adaptive fusion to select such information.

Fig.4 shows the framework of adaptive fusion in TSSF. Along spatial axes, we use adaptive fusion to merge similar dynamic information from point features belonging to the same time. However, in some situations, pseudo multi-view sequences are generated by Diffusion model with real single-view video as a condition. The quality of pseudo multi-view sequences influences fusion effectiveness. For example, dynamic regions are noticeably obscured in specific viewpoints. Hence, we design two adaptive fusion methods, global awareness fusion (GA) and distance awareness fusion (DA), to cope with different scenarios.

Global awareness (GA). At time i , the fully-connection layer (FC) generates a score map $\mathbf{W} = \{w^{(0,0)}, \dots, w^{(t,v)}\}$ for the point features of each view,

$$\mathbf{W} = \text{Softmax}(\text{FC}(\mathbf{F}_p)). \quad (3)$$

Then, we fuse them into fused point features by the weighted summation of all point features according to their score map. The fused features f_a^i can be calculated as:

$$f_a^i = \sum_{j=0}^v w^{(i,j)} f_p^{(i,j)}. \quad (4)$$

The zones that exhibit similar dynamic information in point features of different viewpoints hold significant weights. Hence, similar dynamic features can be merged.

Distance awareness (DA). In general, the frames of the front view are from real single-view video, and the other views are pseudo. The front frame reveals the relatively intact motion areas of the object at various timestamps compared to the other views. Thus, at time i , we calculate the L_1 distance between point features from the front view and point features from the other views. Then, we append pseudo point features with distance features and merge

them by eq. (3) and eq. (4). The fused pseudo point features are appended to real point features. And we once again merge the features by eq. (3) and eq. (4) to acquire the fused point features f_a^i . Through the above pre-processing feature filtering, we reserve the distance features of the pseudo point features relative to the real point features in advance instead of complete pseudo point features. Thus, we reduce the impact of pseudo frame quality on merging dynamic information.

In addition to fused features we obtained through adaptive fusion, we also present dynamic Gaussian features as 3D Gaussian features with HexPlane [53] for inherently regularizing features of fields and guaranteeing their smoothness. Formally, the dynamic Gaussian features at time i :

$$f_{\text{hg}}^i = \text{HexPlane}(X_i, s_i, \gamma_i, \sigma, \zeta), \quad (5)$$

where $X_i = (x_i, y_i, z_i)$ denotes the position of Gaussian points, s_i and γ_i denote scale and rotation at time i . σ and ζ represent opacity and spherical harmonic coefficients of the radiance. Then, we combine dynamic Gaussian features f_{hg}^i and fused point features f_a^i at time i , and map them to fused Gaussian features via learnable linear transformation. The fused Gaussian features not only represent Gaussian intrinsic properties but also capture rich dynamic information, essential for 4D generation by accurately predicting deformation using Deformation MLP.

3.5. Training Objectives

Following [1], we calculate SDS loss based on rendered views and ground truth images, including input video and pseudo multi-view images. Furthermore, we compute the photometric loss among them. Considering if we employ photometric loss on the pseudo multi-view images with rendered views, the quality of pseudo multi-view images directly impacts optimization on pixel-level. Therefore, we introduce the LPIPS loss [54] widely used in 3D generation [19, 55, 56] to minimize the similarity between pseudo multi-view images and rendered views. More details can be found in the supplementary material.

4. Experiments

4.1. Implementation Details

The implementation details are provided in the section.

Datasets For a fair quantitative evaluation, we utilize the dataset provided by Consistent4D. Consistent4D dataset includes 7 dynamic objects. Each object contains an input video and four ground truth videos with different camera settings. Additionally, we introduce an extra 7 dynamic objects sampling from a subset of Objaverse [13, 21]. Each object is rendered to 24 input frames with a front camera pose and 24 ground truth frames with 360° cameras. Furthermore, we use a set of videos from online sources for

Methods	Optimization	Consistent4D dataset				Objaverse dataset			
		CLIP \uparrow	LPIPS \downarrow	FVD \downarrow	FID-VID \downarrow	CLIP \uparrow	LPIPS \downarrow	FVD \downarrow	FID-VID \downarrow
Consistent4D [20]	✓	0.9085	0.1316	1041.2242	28.6471	0.8491	0.2222	1814.5652	48.7921
Dreamgaussian4D [48]	✓	0.9145	0.1517	844.9087	37.9977	0.8127	0.2017	1545.3009	58.3686
STAG4D [1]	✓	0.9078	0.1354	986.8271	26.3705	0.8790	0.1811	1061.3582	30.1359
SC4D [16]	✓	0.9117	0.1370	852.9816	26.4779	0.8490	0.1852	1067.7582	40.5130
4Diffusion [11]	✗	0.8734	0.2284	1551.6363	149.6170	-	-	-	-
L4GM [12]	✗	0.9132	0.1587	1360.0434	40.2446	-	-	-	-
DS4D-GA (Ours)	✓	0.9206	0.1311	799.9367	26.1794	0.8868	0.1761	890.2646	26.6717
DS4D-DA (Ours)	✓	0.9225	0.1309	784.0235	24.0492	0.8881	0.1759	870.9489	25.3836

Table 1. Evaluation and comparison of the performance on Consistent4D dataset and Objaverse dataset. The best score is highlighted in bold. All the experiments of the methods are carried out using the code from their official GitHub repository. For a fair comparison, the experiment of and L4GM on Objaverse dataset are disregarded since they are inference-based methods trained on this dataset.

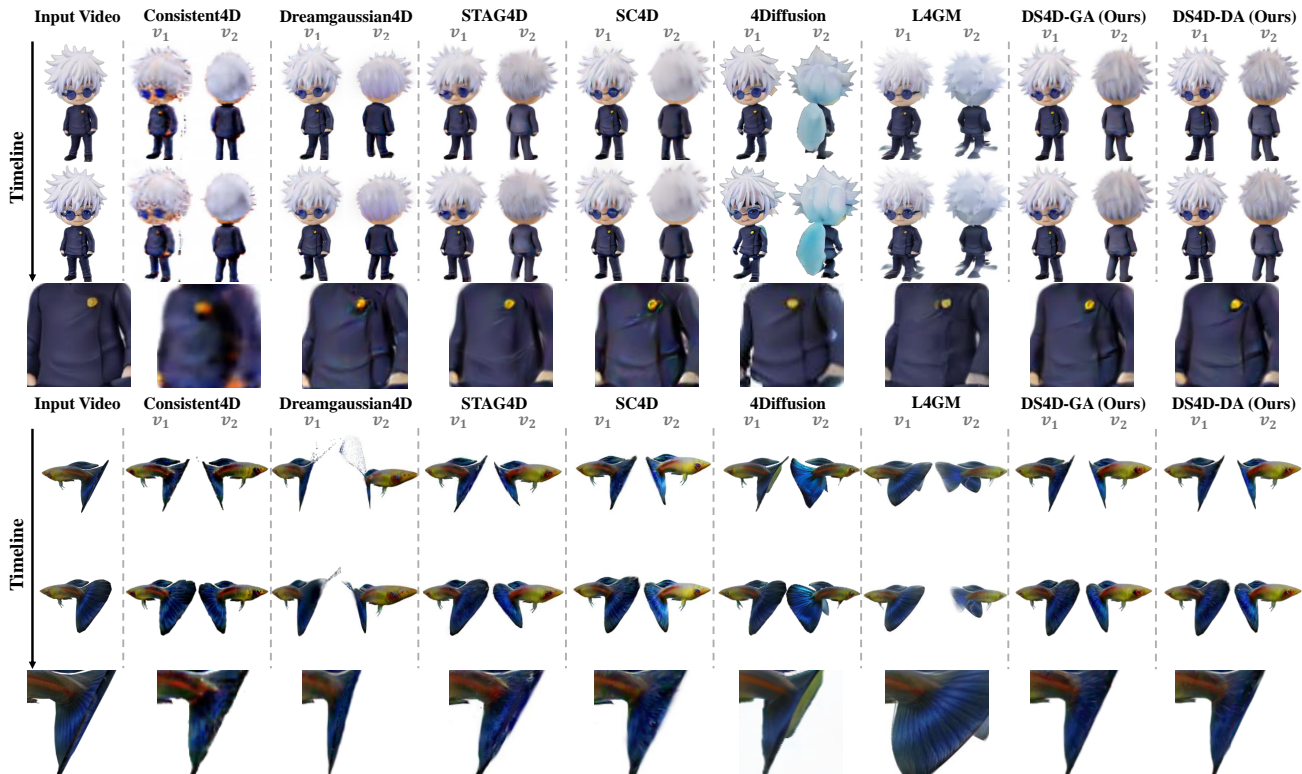


Figure 5. Qualitative comparison on video-to-4D generation. For each method, we render results under two novel views at two timestamps.

qualitative evaluation. In Sec.5, to evaluate the effectiveness of our method in real-world scenarios, we utilize three real-world scenarios provided by Neu3D’s [2] dataset.

Metrics Following Consistent4D [20] and STAG4D [1], we measure the 4D generation quality of our methods using CLIP, LPIPS, FVD and FID-VID. In Sec.5, following [9], we evaluate our results using PSNR, LPIPS, SSIM, and structural dissimilarity index measure (D-SSIM).

Training Our two models, including DS4D-GA (using GA in TSSF) and DS4D-DA (using DA in TSSF) use the same training setting. During the initial 1,000 iterations, we train our models except TSSF and deformation MLP. Sub-

sequently, the models with TSSF and deformation MLP are optimized over 6,000 additional iterations. For the deformation MLP, we employ each MLP with 64 hidden layers and 32 hidden features. The learning rate of TSSF and deformation MLP is set to 1.6×10^{-4} and is decayed to 1.6×10^{-6} . Following [1], the top 2.5% of points are densified with the most accumulated gradient. The overall training process costs approximately 3 hours on a V100 GPU.

4.2. Comparisons with Existing Methods

In this section, we compare our methods DS4D-GA and DS4D-DA with the SOTA methods on Consistent4D

dataset and Objaverse dataset, including Consistent4D [20], Dreamgaussian4D [48], STAG4D [1], SC4D [16], 4Diffusion [11] and L4GM [12]. We conduct qualitative and quantitative comparisons, respectively. The superior performance demonstrates the effectiveness of our methods.

Quantitative comparisons. The quantitative results are shown in Tab. 1. Our methods DS4D-GA and DS4D-DA, consistently outperform other methods in all metrics. Specifically, our methods notably exceed the SOTAs in FVD, indicating that our generation results have fewer temporal artifacts than others. Furthermore, the experiments on Objaverse dataset present that our methods significantly outperform other SOTAs by a large margin. It demonstrates our methods are superior in terms of temporal-spatial consistency, fidelity, and quality of generation results and underscores the robustness of our methods. In summary, such significant improvements are attributed to our method of decoupling dynamic-static features, which can explicitly distinguish dynamic and static zones within frame features.

Qualitative comparisons. The qualitative results on Consistent4D dataset are presented in Fig. 5. Besides, the results on Objaverse dataset are shown in Fig.6. Obviously, whether in the example with a larger proportion of static regions (the person in Fig. 5 and warrior in Fig.6) or the example with a balanced proportion of dynamic and static regions (guppie in Fig. 5), the results, generated by Consistent4D, Dreamgaussian4D, STAG4D and SC4D, have different degrees of blurriness in the details, especially in the areas with motion trends in the current and subsequent frames. Although 4Diffusion and L4GM generate videos with clearer textures than other previous methods with the help of a large amount of 4D data prior, it is easy to generate the abnormal shape or textures with inconsistent details in some areas (e.g, the back of the person). These methods do not differentiate between dynamic and static information, leading them to easily overlook information in dynamic regions when faced with large proportions of static. In contrast, our methods address the challenges arising from varying proportions of dynamic and static regions in frames, leading to the achievement of high-quality 4D generation.

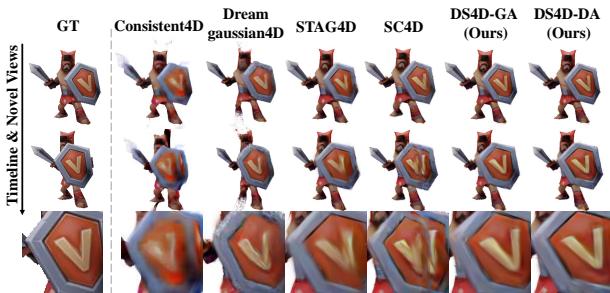


Figure 6. Qualitative comparison on video-to-4D generation based on Objaverse dataset.

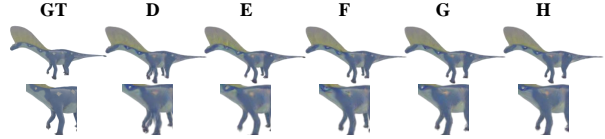


Figure 7. Ablation on different experiment settings from Tab.2.

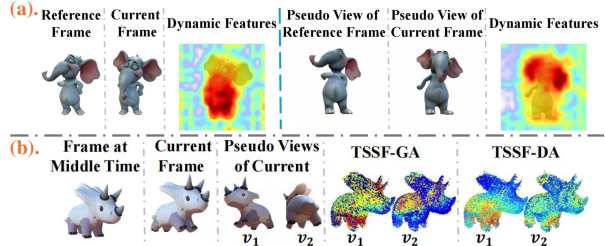


Figure 8. (a) Visualization on the heatmap of dynamic features in DSFD. The red region highlights the primary zone of interest in dynamic features. (b) The score map of point features in TSSF-GA and TSSF-DA. The red area indicates high attention to dynamic information in point features of a specific view.

4.3. Ablation Experiments

To evaluate the effectiveness of different components in our methods, we conduct ablation experiments on Consistent4D and Objaverse datasets as shown in Tab.2. More analysis can be found in supplementary material.

Effect of DSFD. To validate the effect of DSFD, we conduct experiments in two aspects: a) Adding frame features in model (labeled as D). b) Performing decoupling on frame features in model (labeled as E, also termed DSFD). In particular, the performance of D and E both have significant improvement compared to A and B, especially FVD score. For D, the frame features provide enough structure prior knowledge and texture information for Deformation MLP. It assists Deformation MLP in capturing shape deformation. Nevertheless, D fails to differentiate between dynamic and static regions of frames clearly. Consequently, D is prone to overfitting in static areas, resulting in blurry details. For example, the blurred details of legs from D in Fig.7. In contrast, DSFD which decouples dynamic-static features, mitigates the issue.

Effect of TSSF. To validate the effect of TSSF, we add the TSSF based on model E, including model F, G (TSSF-GA) and H (TSSF-DA). Among them, we replace adaptive fusion with average pooling in model F. Specifically, we observe that E, G, H can generate more texture details than other models. Because they mitigate the problem brought by spatial occlusion by aggregating dynamic components from different viewpoints. However, F only averages the point features from DSFD along spatial axes, which ignores merging similar dynamic information. The model G and F adaptively select dynamic information, which plays a cru-

Methods	Point Initialization	Consistent4D dataset				Objaverse dataset			
		CLIP \uparrow	LPIPS \downarrow	FVD \downarrow	FID-VID \downarrow	CLIP \uparrow	LPIPS \downarrow	FVD \downarrow	FID-VID \downarrow
A	✗	0.9133	0.1341	953.6300	27.3747	0.8736	0.1816	1072.1292	28.2410
B	✓	0.9151	0.1313	913.371	27.1357	0.8763	0.1801	1062.9398	28.0977
C. w/ LPIPS Loss	✓	0.9163	0.1311	899.5714	27.0836	0.8773	0.1804	1016.2576	27.8062
D. w/ Frame Features	✓	0.9174	0.1350	888.6579	26.8486	0.8805	0.1778	1005.7503	27.6334
E. w/ DSFD	✓	0.9186	0.1333	861.6075	26.5403	0.8827	0.1765	989.0834	26.9199
F. w/ TSSF-Average Pooling	✓	0.9194	0.1313	839.6600	26.5071	0.8848	0.1761	951.9127	26.8412
G. w/ TSSF-GA (Ours)	✓	0.9206	0.1311	799.9367	26.1794	0.8868	0.1761	890.2646	26.6717
H. w/ TSSF-DA (Ours)	✓	0.9225	0.1309	784.0235	24.0492	0.8881	0.1759	870.9489	25.3836

Table 2. The ablation experiments on Consistent4D dataset and Objaverse dataset. Each setup is based on a modification of the immediately preceding setups. The best score is highlighted in bold.

cial role in enhancing dynamic representations. Compared with E, the texture of 4D content generated by F and H is more refined in Fig.7. This underscores the efficacy of TSSF, including TSSF-GA and TSSF-DA.

4.4. Visualization

In this section, we perform several visualizations of features in DSFD and TSSF, respectively.

Decoupled in DSFD. Fig.8 (a) presents the heatmap of dynamic features obtained by DSFD decoupling features from the current and reference frame features. The red area indicates the primary region of interest in the features. We observe the motion trends come from the trunk and body of elephant in the front view (left of the figure). Thus, dynamic features show strong concern in this area. Limited to the viewpoint range, the motion trajectory for pseudo views (right of the figure) is more interested in the elephant’s head. No doubt, dynamic features also present a high response in similar areas. In conclusion, our method can acquire accurate dynamic features using DSFD, as supported by the visualization results.

Selected in TSSF. Fig.8 (b) shows the score map of selecting similarity dynamic information from point features of different views by TSSF-GA and TSSF-DA. Specifically, the leg movements of the triceratops indicate the primary trend in motion between the middle and current time. The red area indicates the high attention to dynamic information in point features of a specific view. Meanwhile, this area is also similar to the dynamic area of other views in Fig.8 (b). Hence, it reveals that the two approaches can capture a certain degree of similar dynamic information from different viewpoints. However, TSSF-GA is interested in the back of triceratops rather than legs since the front legs are nearly invisible in the pseudo views v_2 . The unseen dynamic region in pseudo view influences the accuracy of selecting similar dynamic information. In contrast, TSSF-DA predicts highest scores on the legs under view v_1 and v_2 , thanks to reducing the impact of pseudo views in TSSF-DA. It indicates TSSF-DA can alleviate issues caused by pseudo views.

Method	PSNR \uparrow	SSIM \uparrow	D-SSIM \downarrow	LPIPS \downarrow
4D-GS [9]	32.1598	0.9483	0.0132	0.1422
Ours	32.3964	0.9494	0.0123	0.1434

Table 3. Evaluation of the performance on Neu3D’s dataset.



Figure 9. Visualization of flame steak compared with 4D-GS.

5. Discussion on Real-World Scenario

Generating a dynamic scene from input real-world videos is an essential task. In this section, we conduct experiments on three scenes from Neu3D’s dataset to demonstrate the effectiveness of our proposed on real-world dynamic scene. We set 4D-GS [9] as the baseline, which has shown promising results in this task. To fair comparison, we directly insert our DSFD and TSSF into 4D-GS. More details can be found in supplementary material.

The results are shown in Tab.3 and Fig.9. Our method achieves competitive results, demonstrating significant potential even for intricate real-world scenarios. Due to static nature of a significant portion of the real-world scene, the previous method easily encounters challenges in exploring dynamic regions, consequently impacting the quality of outputs. Hence, it is necessary to decompose dynamic and

static regions to mitigate this issue. In essence, significant differences exhibit texture variations and motion trends between frames. Thus it is beneficial to utilize this nature to decouple dynamic-static information at feature-level, which enables us to enhance fine-grained dynamic representations. Indeed, there are additional methods available to decouple effectively. For instance, we can introduce optical flow and utilize 3D-aware foundation model [57, 58] to extract depth features used to decouple.

6. Conclusion and Limitations

In this paper, we propose a novel framework DS4D, which decouples dynamic-static information along temporal-spatial axes to enhance dynamic representations for high-quality 4D generation. Its DSFD decouples features by regarding the portions of current features that possess significant differences relative to reference frame features as dynamic features. Moreover, TSSF is designed to enhance dynamic representations by selecting similar dynamic information. Overall, our method can produce high-quality 4D content and shows promise in 4D scene generation.

Limitations. There are several limitations in our method.

1) Since our DS4D relies on multi-view diffusion, e.g., zero123++ [18], the quality of pseudo multi-view sequences still influence our generation results (More experiments and analysis can be found in supplementary material). 2) Limited to the resolution of input video, it is challenge for our method to produce high-resolution 4D contents, e.g., over 2K resolution.

Acknowledgements This work is supported by the National Key Research and Development Plan under Grant 2021YFE0205700, Science and Technology Development Fund of Macau project 0070/2020/AMJ, 00123/2022/A3, 0096/2023/RIA2.

References

- [1] Yifei Zeng, Yanqin Jiang, Siyu Zhu, Yuanxun Lu, Youtian Lin, Hao Zhu, Weiming Hu, Xun Cao, and Yao Yao. Stag4d: Spatial-temporal anchored generative 4d gaussians. *arXiv preprint arXiv:2403.14939*, 2024.
- [2] Tianye Li, Mira Slavcheva, Michael Zollhoefer, Simon Green, Christoph Lassner, Changil Kim, Tanner Schmidt, Steven Lovegrove, Michael Goesele, Richard Newcombe, et al. Neural 3d video synthesis from multi-view video. In *Proceedings of the IEEE/CVF Conference on Computer Vision and Pattern Recognition*, pages 5521–5531, 2022.
- [3] Ruizhi Shao, Zerong Zheng, Hanzhang Tu, Boning Liu, Hongwen Zhang, and Yebin Liu. Tensor4d: Efficient neural 4d decomposition for high-fidelity dynamic reconstruction and rendering. In *Proceedings of the IEEE/CVF Conference on Computer Vision and Pattern Recognition*, pages 16632–16642, 2023.
- [4] Zhengqi Li, Simon Niklaus, Noah Snavely, and Oliver Wang. Neural scene flow fields for space-time view synthesis of dynamic scenes. In *Proceedings of the IEEE/CVF Conference on Computer Vision and Pattern Recognition*, pages 6498–6508, 2021.
- [5] Albert Pumarola, Enric Corona, Gerard Pons-Moll, and Francesc Moreno-Noguer. D-nerf: Neural radiance fields for dynamic scenes. In *Proceedings of the IEEE/CVF Conference on Computer Vision and Pattern Recognition*, pages 10318–10327, 2021.
- [6] Keunhong Park, Utkarsh Sinha, Peter Hedman, Jonathan T Barron, Sofien Bouaziz, Dan B Goldman, Ricardo Martin-Brualla, and Steven M Seitz. Hypernerf: A higher-dimensional representation for topologically varying neural radiance fields. *arXiv preprint arXiv:2106.13228*, 2021.
- [7] Hang Gao, Ruilong Li, Shubham Tulsiani, Bryan Russell, and Angjoo Kanazawa. Monocular dynamic view synthesis: A reality check. *Advances in Neural Information Processing Systems*, 35:33768–33780, 2022.
- [8] Zhiqi Li, Yiming Chen, and Peidong Liu. Dreammesh4d: Video-to-4d generation with sparse-controlled gaussian-mesh hybrid representation. *arXiv preprint arXiv:2410.06756*, 2024.
- [9] Guanjun Wu, Taoran Yi, Jiemin Fang, Lingxi Xie, Xiaopeng Zhang, Wei Wei, Wenyu Liu, Qi Tian, and Xinggang Wang. 4d gaussian splatting for real-time dynamic scene rendering. In *Proceedings of the IEEE/CVF Conference on Computer Vision and Pattern Recognition*, pages 20310–20320, 2024.
- [10] Yiming Xie, Chun-Han Yao, Vikram Voleti, Huaizu Jiang, and Varun Jampani. Sv4d: Dynamic 3d content generation with multi-frame and multi-view consistency. *arXiv preprint arXiv:2407.17470*, 2024.
- [11] Haiyu Zhang, Xinyuan Chen, Yaohui Wang, Xihui Liu, Yunhong Wang, and Yu Qiao. 4diffusion: Multi-view video diffusion model for 4d generation. *arXiv preprint arXiv:2405.20674*, 2024.
- [12] Jiawei Ren, Kevin Xie, Ashkan Mirzaei, Hanxue Liang, Xiaohui Zeng, Karsten Kreis, Ziwei Liu, Antonio Torralba, Sanja Fidler, Seung Wook Kim, et al. L4gm: Large 4d gaussian reconstruction model. *The Thirty-eighth Annual Conference on Neural Information Processing Systems*, 2024.
- [13] Hanwen Liang, Yuyang Yin, Dejia Xu, Hanxue Liang, Zhangyang Wang, Konstantinos N Plataniotis, Yao Zhao, and Yunchao Wei. Diffusion4d: Fast spatial-temporal consistent 4d generation via video diffusion models. *arXiv preprint arXiv:2405.16645*, 2024.
- [14] Uriel Singer, Shelly Sheynin, Adam Polyak, Oron Ashual, Iurii Makarov, Filippos Kokkinos, Naman Goyal, Andrea Vedaldi, Devi Parikh, Justin Johnson, et al. Text-to-4d dynamic scene generation. *arXiv preprint arXiv:2301.11280*, 2023.
- [15] Yuyang Yin, Dejia Xu, Zhangyang Wang, Yao Zhao, and Yunchao Wei. 4dgen: Grounded 4d content generation with spatial-temporal consistency. *arXiv preprint arXiv:2312.17225*, 2023.

- [16] Zijie Wu, Chaohui Yu, Yanqin Jiang, Chenjie Cao, Fan Wang, and Xiang Bai. Sc4d: Sparse-controlled video-to-4d generation and motion transfer. *arXiv preprint arXiv:2404.03736*, 2024.
- [17] Ruoshi Liu, Rundi Wu, Basile Van Hoorick, Pavel Tokmakov, Sergey Zakharov, and Carl Vondrick. Zero-1-to-3: Zero-shot one image to 3d object. In *Proceedings of the IEEE/CVF international conference on computer vision*, pages 9298–9309, 2023.
- [18] Ruoxi Shi, Hansheng Chen, Zhuoyang Zhang, Minghua Liu, Chao Xu, Xinyue Wei, Linghao Chen, Chong Zeng, and Hao Su. Zero123++: a single image to consistent multi-view diffusion base model. *arXiv preprint arXiv:2310.15110*, 2023.
- [19] Jiale Xu, Weihao Cheng, Yiming Gao, Xintao Wang, Shenghua Gao, and Ying Shan. Instantmesh: Efficient 3d mesh generation from a single image with sparse-view large reconstruction models. *arXiv preprint arXiv:2404.07191*, 2024.
- [20] Yanqin Jiang, Li Zhang, Jin Gao, Weiming Hu, and Yao Yao. Consistent4d: Consistent 360° dynamic object generation from monocular video. In *The Twelfth International Conference on Learning Representations*, 2024.
- [21] Matt Deitke, Dustin Schwenk, Jordi Salvador, Luca Weihs, Oscar Michel, Eli VanderBilt, Ludwig Schmidt, Kiana Ehsani, Aniruddha Kembhavi, and Ali Farhadi. Objaverse: A universe of annotated 3d objects. In *Proceedings of the IEEE/CVF Conference on Computer Vision and Pattern Recognition*, pages 13142–13153, 2023.
- [22] Maxime Oquab, Timothée Darcet, Théo Moutakanni, Huy Vo, Marc Szafraniec, Vasil Khalidov, Pierre Fernandez, Daniel Haziza, Francisco Massa, Alaaeldin El-Nouby, et al. Dinov2: Learning robust visual features without supervision. *arXiv preprint arXiv:2304.07193*, 2023.
- [23] Christopher B Choy, Danfei Xu, JunYoung Gwak, Kevin Chen, and Silvio Savarese. 3d-r2n2: A unified approach for single and multi-view 3d object reconstruction. In *European conference on computer vision*, pages 628–644. Springer, 2016.
- [24] Haozhe Xie, Hongxun Yao, Shengping Zhang, Shangchen Zhou, and Wenxiu Sun. Pix2vox++: Multi-scale context-aware 3d object reconstruction from single and multiple images. *International Journal of Computer Vision*, 128(12):2919–2935, 2020.
- [25] Zhenwei Zhu, Liying Yang, Ning Li, Chaohao Jiang, and Yanyan Liang. Umiformer: Mining the correlations between similar tokens for multi-view 3d reconstruction. In *Proceedings of the IEEE/CVF International Conference on Computer Vision*, pages 18226–18235, 2023.
- [26] Liying Yang, Zhenwei Zhu, Xuxin Lin, Jian Nong, and Yanyan Liang. Long-range grouping transformer for multi-view 3d reconstruction. In *Proceedings of the IEEE/CVF International Conference on Computer Vision*, pages 18257–18267, 2023.
- [27] Nanyang Wang, Yinda Zhang, Zhuwen Li, Yanwei Fu, Wei Liu, and Yu-Gang Jiang. Pixel2mesh: Generating 3d mesh models from single rgb images. In *Proceedings of the European conference on computer vision (ECCV)*, pages 52–67, 2018.
- [28] Michael Niemeyer, Lars Mescheder, Michael Oechsle, and Andreas Geiger. Differentiable volumetric rendering: Learning implicit 3d representations without 3d supervision. In *Proceedings of the IEEE/CVF Conference on Computer Vision and Pattern Recognition*, pages 3504–3515, 2020.
- [29] Chao Wen, Yinda Zhang, Chenjie Cao, Zhuwen Li, Xiangyang Xue, and Yanwei Fu. Pixel2mesh++: 3d mesh generation and refinement from multi-view images. *IEEE Transactions on Pattern Analysis and Machine Intelligence*, 45(2):2166–2180, 2022.
- [30] Matheus Gadelha, Rui Wang, and Subhansu Maji. Multiresolution tree networks for 3d point cloud processing. In *Proceedings of the European Conference on Computer Vision (ECCV)*, pages 103–118, 2018.
- [31] Panos Achlioptas, Olga Diamanti, Ioannis Mitliagkas, and Leonidas Guibas. Learning representations and generative models for 3d point clouds. In *International conference on machine learning*, pages 40–49. PMLR, 2018.
- [32] Shitong Luo and Wei Hu. Diffusion probabilistic models for 3d point cloud generation. In *Proceedings of the IEEE/CVF conference on computer vision and pattern recognition*, pages 2837–2845, 2021.
- [33] Ben Mildenhall, Pratul P Srinivasan, Matthew Tancik, Jonathan T Barron, Ravi Ramamoorthi, and Ren Ng. Nerf: Representing scenes as neural radiance fields for view synthesis. *Communications of the ACM*, 65(1):99–106, 2021.
- [34] Thomas Müller, Alex Evans, Christoph Schied, and Alexander Keller. Instant neural graphics primitives with a multiresolution hash encoding. *ACM transactions on graphics (TOG)*, 41(4):1–15, 2022.
- [35] Bernhard Kerbl, Georgios Kopanas, Thomas Leimkühler, and George Drettakis. 3d gaussian splatting for real-time radiance field rendering. *ACM Trans. Graph.*, 42(4):139–1, 2023.
- [36] Zehao Yu, Anpei Chen, Binbin Huang, Torsten Sattler, and Andreas Geiger. Mip-splatting: Alias-free 3d gaussian splatting. In *Proceedings of the IEEE/CVF Conference on Computer Vision and Pattern Recognition*, pages 19447–19456, 2024.
- [37] Chitwan Saharia, William Chan, Saurabh Saxena, Lala Li, Jay Whang, Emily L Denton, Kamyar Ghasemipour, Raphael Gontijo Lopes, Burcu Karagol Ayan, Tim Salimans, et al. Photorealistic text-to-image diffusion models with deep language understanding. *Advances in neural information processing systems*, 35:36479–36494, 2022.
- [38] Ben Poole, Ajay Jain, Jonathan T. Barron, and Ben Mildenhall. Dreamfusion: Text-to-3d using 2d diffusion. In *The Eleventh International Conference on Learning Representations*, 2023.
- [39] Jiayang Tang, Jiawei Ren, Hang Zhou, Ziwei Liu, and Gang Zeng. Dreamgaussian: Generative gaussian splatting for efficient 3d content creation. In *The Twelfth International Conference on Learning Representations*, 2024.

- [40] Keunhong Park, Utkarsh Sinha, Jonathan T Barron, Sofien Bouaziz, Dan B Goldman, Steven M Seitz, and Ricardo Martin-Brualla. Nerfies: Deformable neural radiance fields. In *Proceedings of the IEEE/CVF International Conference on Computer Vision*, pages 5865–5874, 2021.
- [41] Edgar Tretschk, Ayush Tewari, Vladislav Golyanik, Michael Zollhöfer, Christoph Lassner, and Christian Theobalt. Non-rigid neural radiance fields: Reconstruction and novel view synthesis of a dynamic scene from monocular video. In *Proceedings of the IEEE/CVF International Conference on Computer Vision*, pages 12959–12970, 2021.
- [42] Tianhao Wu, Fangcheng Zhong, Andrea Tagliasacchi, Forrester Cole, and Cengiz Oztireli. D²nerf: Self-supervised decoupling of dynamic and static objects from a monocular video. *Advances in neural information processing systems*, 35:32653–32666, 2022.
- [43] Jiemin Fang, Taoran Yi, Xinggang Wang, Lingxi Xie, Xiaopeng Zhang, Wenyu Liu, Matthias Nießner, and Qi Tian. Fast dynamic radiance fields with time-aware neural voxels. In *SIGGRAPH Asia 2022 Conference Papers*, pages 1–9, 2022.
- [44] Zhan Li, Zhang Chen, Zhong Li, and Yi Xu. Spacetime gaussian feature splatting for real-time dynamic view synthesis. In *Proceedings of the IEEE/CVF Conference on Computer Vision and Pattern Recognition*, pages 8508–8520, 2024.
- [45] Yiqing Liang, Numair Khan, Zhengqin Li, Thu Nguyen-Phuoc, Douglas Lanman, James Tompkin, and Lei Xiao. Gaufré: Gaussian deformation fields for real-time dynamic novel view synthesis. *arXiv preprint arXiv:2312.11458*, 2023.
- [46] Jonathon Luiten, Georgios Kopanas, Bastian Leibe, and Deva Ramanan. Dynamic 3d gaussians: Tracking by persistent dynamic view synthesis. In *2024 International Conference on 3D Vision (3DV)*, pages 800–809. IEEE, 2024.
- [47] Zeyu Yang, Hongye Yang, Zijie Pan, and Li Zhang. Real-time photorealistic dynamic scene representation and rendering with 4d gaussian splatting. *arXiv preprint arXiv:2310.10642*, 2023.
- [48] Jiawei Ren, Liang Pan, Jiaxiang Tang, Chi Zhang, Ang Cao, Gang Zeng, and Ziwei Liu. Dreamgaussian4d: Generative 4d gaussian splatting. *arXiv preprint arXiv:2312.17142*, 2023.
- [49] Mohamed El Banani, Amit Raj, Kevis-Kokitsi Maninis, Abhishek Kar, Yuanzhen Li, Michael Rubinstein, Deqing Sun, Leonidas Guibas, Justin Johnson, and Varun Jampani. Probing the 3d awareness of visual foundation models. In *Proceedings of the IEEE/CVF Conference on Computer Vision and Pattern Recognition*, pages 21795–21806, 2024.
- [50] Robin Rombach, Andreas Blattmann, Dominik Lorenz, Patrick Esser, and Björn Ommer. High-resolution image synthesis with latent diffusion models. In *Proceedings of the IEEE/CVF conference on computer vision and pattern recognition*, pages 10684–10695, 2022.
- [51] Alec Radford, Jong Wook Kim, Chris Hallacy, Aditya Ramesh, Gabriel Goh, Sandhini Agarwal, Girish Sastry, Amanda Askell, Pamela Mishkin, Jack Clark, et al. Learning transferable visual models from natural language supervision. In *International conference on machine learning*, pages 8748–8763. PMLR, 2021.
- [52] Luke Melas-Kyriazi, Christian Rupprecht, and Andrea Vedaldi. Pc2: Projection-conditioned point cloud diffusion for single-image 3d reconstruction. In *Proceedings of the IEEE/CVF Conference on Computer Vision and Pattern Recognition*, pages 12923–12932, 2023.
- [53] Ang Cao and Justin Johnson. Hexplane: A fast representation for dynamic scenes. In *Proceedings of the IEEE/CVF Conference on Computer Vision and Pattern Recognition*, pages 130–141, 2023.
- [54] Richard Zhang, Phillip Isola, Alexei A Efros, Eli Shechtman, and Oliver Wang. The unreasonable effectiveness of deep features as a perceptual metric. In *Proceedings of the IEEE conference on computer vision and pattern recognition*, pages 586–595, 2018.
- [55] Yicong Hong, Kai Zhang, Jiuxiang Gu, Sai Bi, Yang Zhou, Difan Liu, Feng Liu, Kalyan Sunkavalli, Trung Bui, and Hao Tan. Lrm: Large reconstruction model for single image to 3d. *arXiv preprint arXiv:2311.04400*, 2023.
- [56] Zi-Xin Zou, Zhipeng Yu, Yuan-Chen Guo, Yangguang Li, Ding Liang, Yan-Pei Cao, and Song-Hai Zhang. Triplane meets gaussian splatting: Fast and generalizable single-view 3d reconstruction with transformers. In *Proceedings of the IEEE/CVF Conference on Computer Vision and Pattern Recognition*, pages 10324–10335, 2024.
- [57] Haofei Xu, Songyou Peng, Fangjinhua Wang, Hermann Blum, Daniel Barath, Andreas Geiger, and Marc Pollefeys. Depthspat: Connecting gaussian splatting and depth. *arXiv preprint arXiv:2410.13862*, 2024.
- [58] Lihe Yang, Bingyi Kang, Zilong Huang, Zhen Zhao, Xiao-gang Xu, Jiashi Feng, and Hengshuang Zhao. Depth anything v2. *arXiv preprint arXiv:2406.09414*, 2024.